Transp Porous Med (2007) 67:453–471
DOI 10.1007/s11242-006-9036-9

ORIGINAL PAPER

Forced convection of gaseous slip-flow in porous micro-channels under Local Thermal Non-Equilibrium conditions

O. M. Haddad · M. A. Al-Nimr · J. Sh. Al-Omary

Received: 7 March 2005 / Accepted: 4 July 2006 / Published online: 1 September 2006

Abstract Steady laminar forced convection gaseous slip-flow through parallel-plates micro-channel filled with porous medium under Local Thermal Non-Equilibrium (LTNE) condition is studied numerically. We consider incompressible Newtonian gas flow, which is hydrodynamically fully developed while thermally is developing. The Darcy–Brinkman–Forchheimer model embedded in the Navier–Stokes equations is used to model the flow within the porous domain. The present study reports the effect of several operating parameters on velocity slip and temperature jump at the wall. Mainly, the current study demonstrates the effects of: Knudsen number (Kn), Darcy number (Da), Forchheimer number (Γ), Peclet number (Pe), Biot number (Bi), and effective thermal conductivity ratio (K_R) on velocity slip and temperature jump at the wall. Results are given in terms of skin friction ($C_f Re^*$) and Nusselt number (Nu). It is found that the skin friction: (1) increases as Darcy number increases; (2) decreases as Forchheimer number or Knudsen number increases. Heat transfer is found to (1) decreases as the Knudsen number, Forchheimer number, or K_R increases; (2) increases as the Peclet number, Darcy number, or Biot number increases.

Keywords Forced convection · Slip-flow · Porous media · Micro-channel · Graetz problem · Local thermal non-equilibrium

Nomenclature

Bi	Biot number ($h_{sf}L^2/\varepsilon k_f$)
c_f	Coefficient in the Forchheimer term
C_f	Skin friction coefficient
C_p	Constant pressure specific heat

O. M. Haddad (✉) · M. A. Al-Nimr · J. Sh. Al-Omary
Department of Mechanical Engineering,
Jordan University of Science and Technology,
P.O. Box 3030, Irbid 22110, Jordan
e-mail: haddad@just.edu.jo

C_v Constant volume specific heat
D Pore diameter
Da Darcy number $(K/\varepsilon L^2)$
h Local heat transfer coefficient
h_{sf} Interstitial heat transfer coefficient
k Thermal conductivity
K Intrinsic permeability of the porous medium
Kn Modified Knudsen number $\left(\frac{\lambda}{D}\,\frac{D}{L}\right)$
K_{R} Effective thermal conductivity ratio $(\varepsilon k_{\mathrm{f}}/(1-\varepsilon)k_{\mathrm{s}})$
L Half channel width
Nu Nusselt number $(hL/\varepsilon k_{\mathrm{f}})$
p Pressure
Pe Peclet number $(u_{\mathrm{o}}L/\varepsilon\alpha)$
Pr Prandtl number $(\mu/\alpha\rho_{\mathrm{f}})$
q_{w} Heat transfer rate from the plate wall
Re^* Modified Reynolds number in porous media $(\rho_{\mathrm{f}}u_o L/\mu\varepsilon)$
t Time
t_0 Reference time $(\rho L^2/\mu)$
T Temperature
u Axial velocity
u_0 Reference axial velocity $(\varepsilon L^2/\mu(-\mathrm{d}p/\mathrm{d}x))$
U Non-dimensional axial velocity (u/u_{o})
x Axial coordinate
X Dimensionless axial coordinate (x/L)
y Transverse coordinate
Y Dimensionless transverse coordinate (y/L)

Greek symbols
α Thermal diffusivity
γ Specific heat ratio (C_p/C_v)
Γ Dimensionless coefficient of Forchheimer $(\rho_{\mathrm{f}}c_{\mathrm{f}}\varepsilon^2(-\mathrm{d}p/\mathrm{d}x)L^4/\mu^2\sqrt{k})$
λ Mean free path of the gas molecules
ε Porosity of the porous medium
μ Dynamic viscosity
ρ_{f} Fluid density
σ_{T} Thermal accommodation coefficient
σ_{v} Tangential momentum accommodation coefficient
θ Non-dimensional temperature $(T-T_\infty/T_{\mathrm{w}}-T_\infty)$
τ Non-dimensional time (t/t_{o})
τ_{w} Shear stress at the wall $(-\mu(\partial u/\partial y))|_{\mathrm{w}}$

Subscripts
f Fluid
mf Mean value for the fluid
s Solid
w Wall

1 Introduction

Analysis of fluid flow and heat transfer in a porous medium has been a subject of continuous interest during the past few decades because of its wide range of engineering applications. In addition to conventional applications such as solar receivers, building thermal insulation materials, packed bed heat exchangers, and energy storage units, investigators have found new applications in the emerging field of micro-scale heat transfer. As Bejan (2000) pointed out, this new opportunity stems from the need for smaller flow passages and fins used in compact heat exchangers and electronics cooling.

Various analytical and numerical studies on transport phenomena in porous media are generally based on the assumption of local thermal equilibrium (LTE); that is to say, both the fluid phase and the solid phase are at the same temperature. Under the assumption of LTE, many investigators have used the so-called one-equation model to obtain temperature distributions in a porous medium because an analysis using the one-equation model is simple and straightforward. When the condition of LTE is far from reality, the one-equation model needs to be replaced with the two-equation model, which treats the solid phase and the fluid phase separately. In this study, the two-equation model will be used to analyze the gas flow through parallel plates micro-channel filled with porous medium. Such a porous micro-channel can be used as filter in micro-systems and as a porous micro-heat exchanger in applications where enhancing heat transfer is required by enlarged surface-to-volume ratio due to the existing porous medium.

One of the major difficulties in trying to predict the gaseous transport in micron-sized devices can be attributed to the fact that the continuum flow assumption implemented in the Navier–Stokes equations breaks down when the mean free path of the molecules (λ) is comparable to the characteristic dimension of the flow domain. Under these conditions, the momentum and heat transfer start to be affected by the discrete molecular composition of the gas and a variety of non-continuum or rarefaction effects are likely to be exhibited such as velocity slip and temperature jump at the gas–solid interface. Velocity profiles, fluid flow rate, boundary wall shear stresses, temperature profiles, heat transfer rates, and Nusselt number are all influenced by the non-continuum regime. In addition, the hydrodynamic entrance length of the channel, defined as the downstream distance measured from the channel inlet beyond which the flow velocity profile becomes invariant, may also be affected (Barber and Emerson 2001).

However, there is a certain limit of the channel size with which one can still apply Navier–Stokes equations with some modifications on the boundary conditions (Arkilic et al. 1994; Shih et al. 1996). This is the case when Knudsen number (Kn) is in the range $0.001 \leq \mathrm{Kn} \leq 0.1$, and the flow under such condition is called slip-flow. Knudsen number, defined as the ratio of the mean free path of the molecule to the characteristic length of the channel, is used as a measure of the rarefaction effects in microflows. It also measures the deviation of the fluid behavior from the continuum behavior so that the right flow model is used (Beskok and Karniadakis 1994). The continuum Navier–Stokes equations with no-slip (in velocity)/no-jump (in temperature) boundary conditions are valid as long as the Knudsen number does not exceed 0.001 (called the continuum regime). First-order velocity slip/temperature jump boundary conditions should be applied to the continuum Navier–Stokes equations in the range of $0.001 \leq \mathrm{Kn} \leq 0.1$ (slip-flow regime), which is the focus of the

present study. The transition regime spans the range of $0.1 < \mathrm{Kn} < 10$ and second-order or higher velocity slip/temperature jump boundary conditions are applicable there. Note, however, that the Navier–Stokes equations are first-order accurate in Kn and are themselves not valid in the transition regime. Either higher-order continuum equations, e.g. Burnett equations, should be used there or molecular modeling should be invoked (Gad-El-Hak 1999).

Flows in the slip-flow regime have traditionally been modeled using the Navier–Stokes and energy equations modified by boundary conditions that contain the rarefaction effects on the velocity and temperature fields. Eckert and Drake (1972) have indicated that there is strong evidence to support this approach. More recently, Liu et al. (1995) and Arkilic et al. (1994) found that the Navier–Stokes equations, when combined with slip-flow boundary conditions, yield results for pressure drop and friction factor that are in agreement with experimental data for some micro-channel flows. The Graetz problem considers the developing temperature field in a circular tube for a fluid that is hydrodynamically fully developed. This traditional problem has been modified through the velocity slip and temperature jump boundary conditions to study internal convective heat transfer occurring in circular tubes in the slip-flow regime. Shih et al. (1995), Barron et al. (1996, 1997), and Wang (1996) have investigated this problem for an isothermal wall condition. Their results indicate that the rarefaction effects, manifested as slip-flow at the boundary, augment heat transfer. However, there are two simplifications adopted in those studies that reduce the applicability of the results. First, the temperature jump boundary condition was actually not directly implemented in these solutions. Second, both the thermal-accommodation-coefficient (σ_T) and the tangential-momentum-accommodation coefficient (σ_v) were assumed to be unity. This second assumption, while reasonable for most fluid–solid combinations, produces a solution limited to specific set of fluid–solid conditions. Ameel et al. (1997) studied the related Graetz problem under constant heat flux at the wall. In this case, increasing rarefactions effects produced a reduction in heat transfer. An indirect solution method, which utilizes the eigenvalue problem for the isothermal case, was implemented. On the other hand, Wang et al. (1998) obtained the analytical solution of the extended Graetz problem with constant heat flux wall conditions through a direct solutions method. Once again, the slip effects were shown to reduce heat transfer. In both Ameel et al. (1997) and Wang et al. (1998), the accommodation coefficients were assumed to have values of unity.

A generalized investigation of the extended Graetz problem was considered by Larrode et al. (2000). The effects of rarefaction and the fluid–wall interaction were included through the introduction of two non-dimensional parameters. The results from Larrode et al. (2000) indicate that heat transfer depends both on the degree of rarefaction and on the surface accommodation coefficients. The values of the two non-dimensional parameters were found to influence the heat transfer, which may increase, decrease, or remain unchanged when compared to non-slip-flow. Yu and Ameel (2000) studied slip-flow heat transfer in a microscale gap formed from isothermal surfaces. Contrary to all previous studies, axial conduction effects were included and the results were similar to those of Larrode et al. (2000). However, the inclusion of axial conduction was found to increase heat transfer and the thermal entrance length.

As part of a continued effort by the authors toward understanding the flow in microchannels (e.g., Haddad et al. 2005a, b, 2006a, b), the objective of this study is to investigate the effect of Knudsen, Darcy, Forchheimer, Peclet, Biot numbers, and conduction

coefficient ratio on the hydrodynamically fully developed and thermally developing forced convection gaseous flow in an isothermal parallel-plates micro-channel. The micro-channel is filled with porous medium under LTNE and steady state conditions. The present study is focused on the slip-flow regime ($0.001 \leq \mathrm{Kn} \leq 0.1$) and therefore the boundary conditions are restricted to the first-order velocity slip and temperature jump conditions. Since the channel at hand is symmetric in both geometry and boundary conditions, only one half of the solution domain will be considered.

Momentum and energy transfer between the gas molecules and the surface requires specification of interactions between the impinging gas molecules and the surface. From the macroscopic point of view, it is sufficient to know some average parameters in terms of the so-called tangential momentum (σ_{v}) and thermal (σ_{T}) accommodation coefficients. These coefficients describe the gas–surface interaction and are functions of the composition and temperature of the gas, the gas velocity over the surface, and the solid surface temperature, chemical state, and roughness. The accommodation coefficients take any value between 0 and 1, where these values represent specular reflection and diffuse reflection, respectively. For most engineering applications, values of the accommodation coefficients are near unity (Yu and Ameel 2000). Throughout the present study, the Prandtl number (Pr), gas constant (γ), tangential momentum-accommodation coefficient (σ_{v}), and thermal-accommodation coefficient (σ_{T}) are taken to be 0.7, 1.4, 0.7, and 0.7, respectively, to be in accordance for a common gas flowing in practical micro-channel (Gad-El-Hak 1999).

2 Mathematical formulation

Consider a steady laminar forced convection flow between semi-infinite parallel-plates micro-channel filled with porous medium as shown schematically in Fig. 1. Based on the assumption that the flow is hydrodynamically fully developed, the velocity component in y-direction vanishes and the velocity component in x-direction (denoted by u) is dependent on y only. In addition, the flow is assumed to be thermally developing, under constant pressure gradient driving force, and therefore the temperature is a function of (x, y) only. The present study is focused on the slip-flow regime ($10^{-3} \leq \mathrm{Kn} \leq 10^{-1}$), and therefore the Navier–Stokes and energy equations can be combined with the first-order slip/jump boundary conditions as this would be applicable. The fluid (gas) is assumed to be incompressible, having constant physical properties and under local thermal non-equilibrium condition with the rigid solid

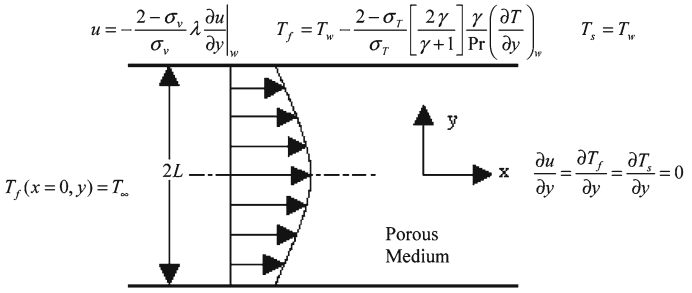

Fig. 1 Schematic diagram of the physical problem

matrix, hence the two equation model will be used to describe the thermal behavior. On the other hand, it is assumed that the porous medium is isotropic, rigid, and homogeneous. Under the above assumptions, and by using the non-dimensional variables listed in the nomenclature, the momentum and energy equations can be reduced to the following form (See Appendix) (Marafie and Vafai 2001):

$$0 = 1 + \frac{\partial^2 U}{\partial Y^2} - \frac{1}{\mathrm{Da}} U - \Gamma U^2 \tag{1}$$

$$\frac{\partial^2 \theta_\mathrm{f}}{\partial Y^2} + \mathrm{Bi}(\theta_\mathrm{s} - \theta_\mathrm{f}) = \mathrm{Pe}\ U \frac{\partial \theta_\mathrm{f}}{\partial X} \tag{2}$$

$$\frac{\partial^2 \theta_\mathrm{s}}{\partial Y^2} + \mathrm{Bi}\ K_\mathrm{R}\ (\theta_\mathrm{f} - \theta_\mathrm{s}) = 0 \tag{3}$$

The current study is focused on the rarefaction effect and therefore compressibility effect is ignored. This is reasonable at relatively low Mach numbers (Ma). Usually, it is difficult for the flow in porous medium to attain high velocities due to the high resistance imposed by the presence of the solid matrix. The low level velocity makes it difficult to attain high Ma flow, and therefore compressibility effect is insignificant. The dimensionless form of the boundary conditions is given as:

$$U(1) = -\frac{2 - \sigma_\mathrm{v}}{\sigma_\mathrm{v}} \mathrm{Kn}\ \left.\frac{\partial U}{\partial Y}\right|_\mathrm{w} \tag{4}$$

$$\theta_\mathrm{f}(X, Y = 1) = 1 - \frac{2 - \sigma_\mathrm{T}}{\sigma_\mathrm{T}} \left[\frac{2\gamma}{\gamma + 1}\right] \frac{\mathrm{Kn}}{\mathrm{Pr}}\ \left.\frac{\partial \theta_\mathrm{f}}{\partial Y}\right|_\mathrm{w} \tag{5}$$

$$\theta_\mathrm{s}(X, Y = 1) = 1 \tag{6}$$

$$\frac{\partial U}{\partial Y}(Y = 0) = \frac{\partial \theta_\mathrm{f}}{\partial Y}(X, Y = 0) = \frac{\partial \theta_\mathrm{s}}{\partial Y}(X, Y = 0) \tag{7}$$

$$\theta_\mathrm{f}(X = 0, Y) = 0 \tag{8}$$

The quantities of primary interest in this study are the friction factor and Nusselt number. These are also defined as follows:

$$C_\mathrm{f} = \frac{|\tau_\mathrm{w}|}{\frac{1}{2}\rho_\mathrm{f}\frac{u_0^2}{\varepsilon^2}} = \frac{\left|\frac{\mu}{\varepsilon}\frac{\partial u}{\partial y}\right|_\mathrm{w}}{\frac{1}{2}\rho_\mathrm{f}\frac{u_0^2}{\varepsilon^2}} = \frac{2}{Re^*}\left|\frac{\mathrm{d}U}{\mathrm{d}Y}\right|_\mathrm{w} \tag{9}$$

$$\mathrm{Nu} = \frac{hL}{\varepsilon k_\mathrm{f}} = \frac{1}{1 - \theta_\mathrm{mf}}\left\{\left.\frac{\partial \theta_\mathrm{f}}{\partial Y}\right|_\mathrm{w} + \frac{1}{K_\mathrm{R}}\left.\frac{\partial \theta_\mathrm{s}}{\partial Y}\right|_\mathrm{w}\right\} \tag{10}$$

3 Numerical method

The governing equations are solved numerically using the finite difference technique. The finite difference equations (FDEs) of the governing partial differential equations (PDEs) are obtained by replacing all derivatives in the PDEs by their respective finite difference approximations. The governing momentum and energy equations are not coupled; consequently the numerical solution proceeds by first solving the momentum equation for the velocity distribution, then the two coupled energy equations are solved for the solid and fluid temperature profiles.

The momentum equation (1) is solved by first adding a fictitious time derivative term into the equation, and then the well-known Backward-Time Centered-Space finite difference method (Hoffman 2001) is used to solve the resulting unsteady equation. This particular method is also called the fully implicit method. The FDE that approximates the PDE is obtained by replacing $\partial U/\partial \tau$ term by its first-order backward-time approximation, and $\partial^2 U/\partial Y^2$ term by its second-order centered-space approximation. The steady state solution is obtained by marching in time until no further significant change in the solution is obtained with additional marching steps. The present numerical method is advantageous over the other available numerical methods in that it is unconditionally stable.

In a similar manner, the energy equations are discretized using the same numerical scheme. In contrast to the momentum equation, the steady state form of the energy equations is discretized directly and therefore a time dependent solution has not been obtained. When the momentum equation (1) is discretized and applied at every point in the finite difference grid, a system of non-linear finite difference (algebraic) equations was obtained. To overcome the difficulties in solving such a system, the non-linear term (last term) in Eq. (1) should be linearized. To do this, the well-known time lagging technique is used. More details on this technique can be found in Hoffman (2001).

Based on the above finite difference scheme, the resulting systems (from the momentum and energy equations) of algebraic equations is tri-diagonal. Such systems are best solved by Thomas algorithm (Hoffman 2001). For the momentum and energy equations, a uniform grid is used in both X- and Y-directions. The adequacy of the grid is verified by successive refinements of grid size until no further change in the solution is observed. For the momentum equation, it is found that a grid size of (100) points in Y-direction would result in accurate solutions and any increase beyond this size would lead to an insignificant change in the resulting solution. Also, the dimensionless time step used is based on number of refinements to ensure an independent solution. It is found that a time step that is equal to 0.1 or smaller would lead to invariant solutions. On the other hand, it is found that a grid size in (X, Y) directions of 200×100 points, respectively, is satisfactory. Thus, a mesh size of 200×100 grid points in X- and Y-directions is used throughout this study.

4 Results and discussion

To verify the current numerical results, Eq. (1) will be solved analytically for a special case: for problems with $\Gamma = 0$ (i.e., negligible microscopic inertial term), Eq. (1) becomes linear and can be easily solved analytically. The obtained solution under such condition is

$$U(Y) = \mathrm{Da}\left[1 + \frac{\cosh\frac{Y}{\sqrt{\mathrm{Da}}}}{\frac{-(2-\sigma_v)\,\mathrm{Kn}}{\sigma_v\sqrt{\mathrm{Da}}}\sinh\frac{1}{\sqrt{\mathrm{Da}}} - \cosh\frac{1}{\sqrt{\mathrm{Da}}}}\right] \tag{11}$$

Figure 2 shows a comparison between the obtained numerical and analytical velocity profiles when $\Gamma = 0$. The comparison shows that there is excellent agreement between the two solutions. Furthermore, the obtained solution by Yu and Ameel (2001) for the case of no-slip-flow in a clear domain is reproduced numerically by the present study. Figure 3 shows that the agreement between the obtained numerical results and the

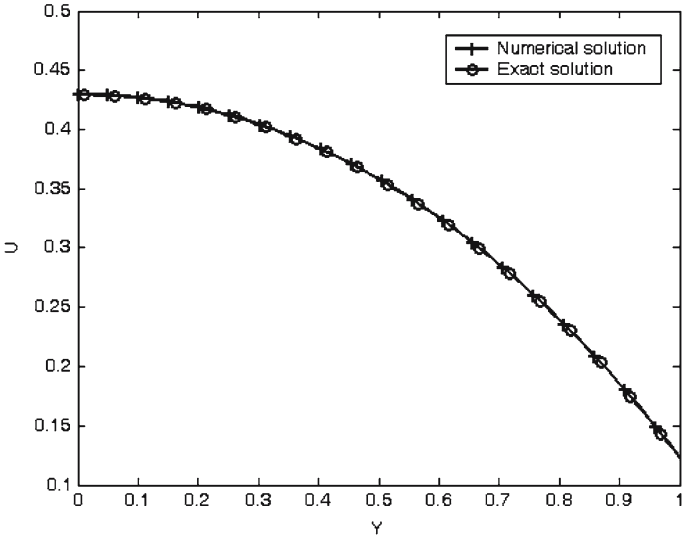

Fig. 2 Comparison between the numerical and analytical velocity profiles: Da $= 1$, $\Gamma = 0$, Kn $= 0.1$

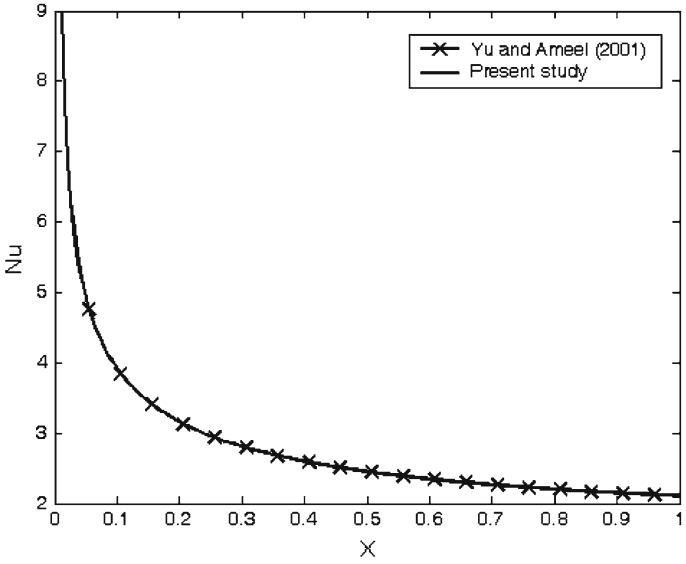

Fig. 3 Comparison of the present study results with Yu and Ameel (2001): Da $= \infty$, $Re = 50$, $\Gamma = 0$, Kn $= 0.0$

published results is very good. Before we proceed, it is important to point out here that our results are shown in terms of the modified Knudsen number (Kn $= \frac{\lambda}{D}\frac{D}{L}$) and are valid provided that $10^{-3} \leq \lambda/D \leq 10^{-1}$.

Figure 4 shows the velocity profile at different Knudsen numbers. From those curves it is clear that as Knudsen number increases, the velocity profile shifts up to show increase in local velocity and so the velocity slip at the channel-wall increases.

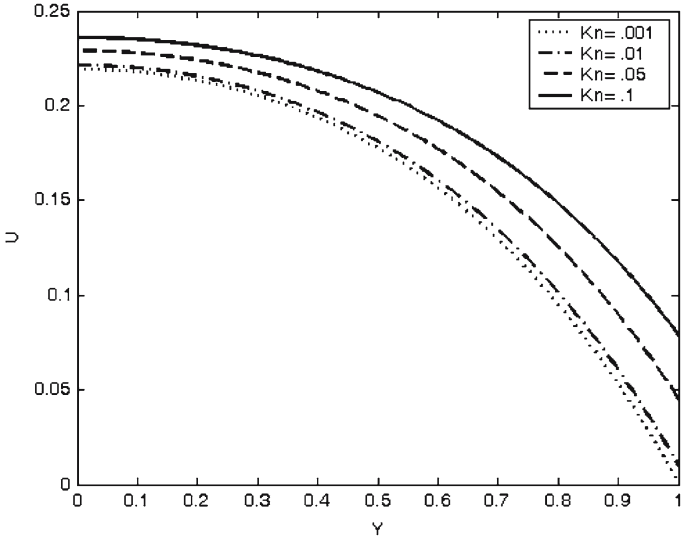

Fig. 4 Effect of Kn on the non-dimensional velocity distribution: Da $= 1$, $\Gamma = 10$

This is because the increase in Knudsen number can be due to increase in the mean free path of the molecules, which in turn decreases the retarding effect at the wall. This yields larger flow rate through the channel but the increase in maximum velocity is not significant compared to that at the channel-wall and so the velocity gradient at the wall decreases with increasing Knudsen number. One can also note that the mass flow rate increases since the pumping force is kept constant while the frictional retarding forces at the wall decrease.

Figures 5 and 6 show the development of the non-dimensional temperature profiles of the fluid and solid at different axial stations, and for different Knudsen numbers. From those figures it can be noted that as Knudsen number increases the non-dimensional temperature profiles θ_f and θ_s shift down. The decrease in θ_f with Kn can be attributed to two effects: (a) increasing Knudsen number means that more flow passes through the channel (i.e., heat source at the wall must heat greater amount of fluid), (b) As Knudsen number increases the jump in the fluid temperature at the wall will increase and this leads to a less amount of heat transfer from the wall to the fluid. The same behavior is true for the solid domain temperature. As Knudsen number increases, the reduction in θ_f curves leads to a reduction in θ_s due to heat transfer from the solid domain to the colder fluid. It can be observed that for any Knudsen number the solid temperature is larger than that of the fluid due to the fact that the solid domain is in perfect thermal contact with the wall and there is no temperature jump between the wall and the adjacent solid material. As a result, the solid domain receives higher heat flux from the wall and consequently it has higher temperature than fluid. One can also observe that the effect of Knudsen number on the non-dimensional temperature is more significant at larger values of Knudsen number. This effect also spreads out to the centerline as we move away from the entrance, and the effect of Knudsen number is more pronounced at the wall near the entrance.

Figure 7 shows the effect of Darcy number on skin friction for different Knudsen numbers. The curves show that as Knudsen number increases, $C_f Re^*$ decreases. It

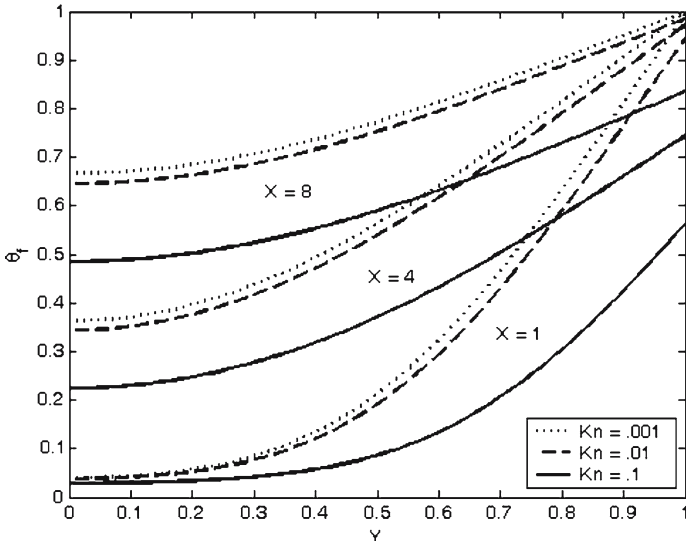

Fig. 5 Effect of Kn on the non-dimensional fluid temperature distribution: Da $= 1, \Gamma = 10$, Pe $= 100$, Bi $= 1$, $K_R = 1$

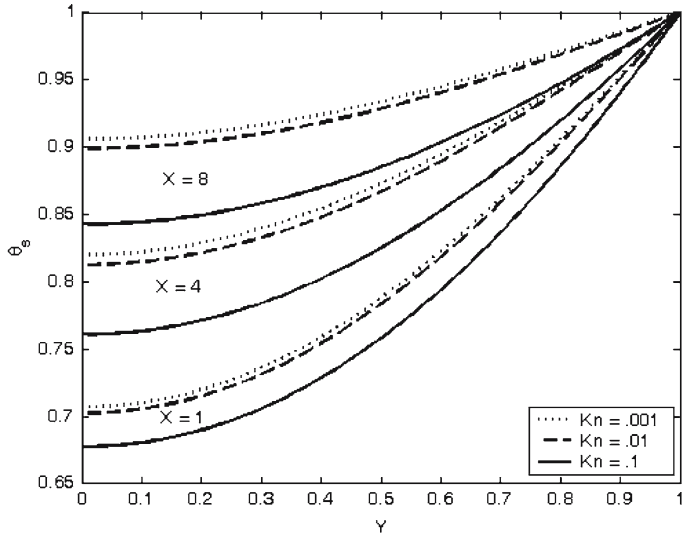

Fig. 6 Effect of Kn on the non-dimensional solid temperature distribution: Da $= 1, \Gamma = 10$, Pe $= 100$, Bi $= 1$, $K_R = 1$

is known that any increase in Knudsen number would result in an increase in Re^* due to the increase in the flow velocity, whereas C_f decreases due to the decrease in velocity gradient at the wall. The net result of the effect of Knudsen number is found to decrease $C_f Re^*$. This means that the reduction in C_f is more significant so that it overcame the increase in Re^*. The effect of Knudsen number on $C_f Re^*$ is more significant at larger values of Knudsen number $0.01 \leq \text{Kn} \leq 0.1$. The effect of Knudsen

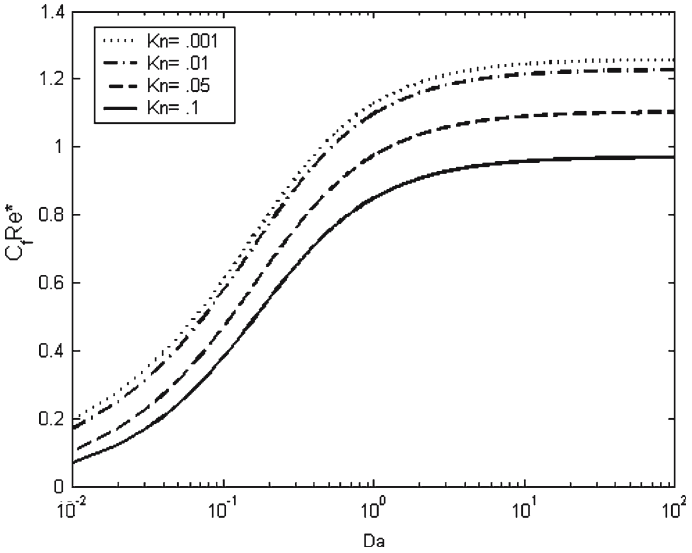

Fig. 7 Variation of $C_f Re^*$ with Da: $\Gamma = 10$

number on $C_f Re^*$ is more significant at larger values of Darcy number, because at larger Darcy number the velocity is relatively higher leading to higher Re^* and much lower C_f values. This implies that any change in Knudsen number at large values of Darcy number would lead to significant change in $C_f Re^*$. The figure shows also that as the Darcy number increases, $C_f Re^*$ increases. This is because as Darcy number increases, permeability of the porous medium increases and therefore more amount of flow enters the channel and higher velocity is attained, which leads to increase in Re^*. The net effect has been found as an increase in $C_f Re^*$ value.

Figure 8 shows the variation of $C_f Re^*$ with Forchheimer number at different Knudsen numbers. The curves show that as Knudsen number increases, $C_f Re^*$ decreases. The effect of Knudsen number on $C_f Re^*$ is more significant at higher values of Knudsen number ($0.01 \leq \text{Kn} \leq 0.1$). Also, these curves show that as the Forchheimer number increases $C_f Re^*$ decreases. Increasing the Forchheimer number decreases both Re^* and C_f. When the Forchheimer number increases, the microscopic inertial retarding force increases. Therefore, the flow velocity is reduced and consequently Re^* is reduced. Also, as Forchheimer number increases, C_f decreases due to the decrease in velocity gradient at the wall and as a result, $C_f Re^*$ will decrease.

Figure 9 shows the effect of Knudsen number on Nusselt number (Nu) over the entire slip-flow regime. As predicted, Nusselt number decreases axially downstream because less heat transfer occurs from the wall to the fluid as the fluid is heated downstream. Farther downstream at large X, the flow becomes thermally developed and Nusselt number value approaches a fixed value. By inspecting Fig. 9, it is clear that as Knudsen number increases, Nusselt number decreases due to the reduction in heat transfer from the wall to the fluid. Increasing Knudsen number has two opposite effects on Nusselt number. The first effect is that it leads to increased velocity slip at the wall as the velocity increases and so larger flow rates are achieved (i.e., larger amount of fluid absorbs heat from the wall), and thus Nusselt number increases. The second effect is that increasing Knudsen number leads to increased temperature jump

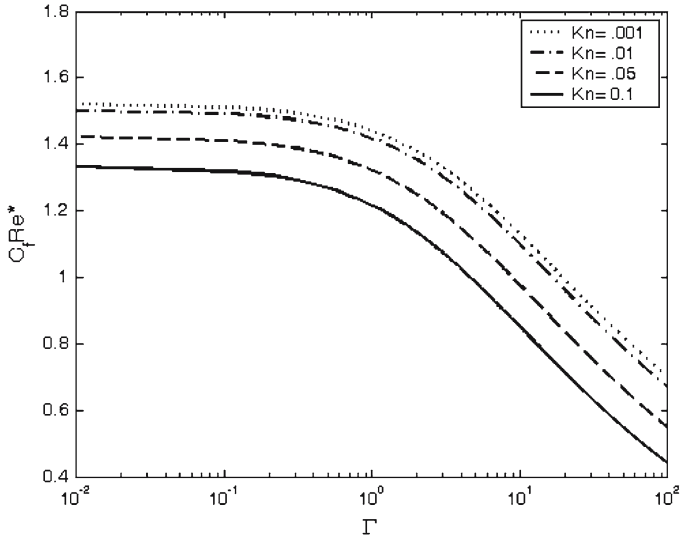

Fig. 8 Variation of $C_f Re^*$ with Γ: Da = 1

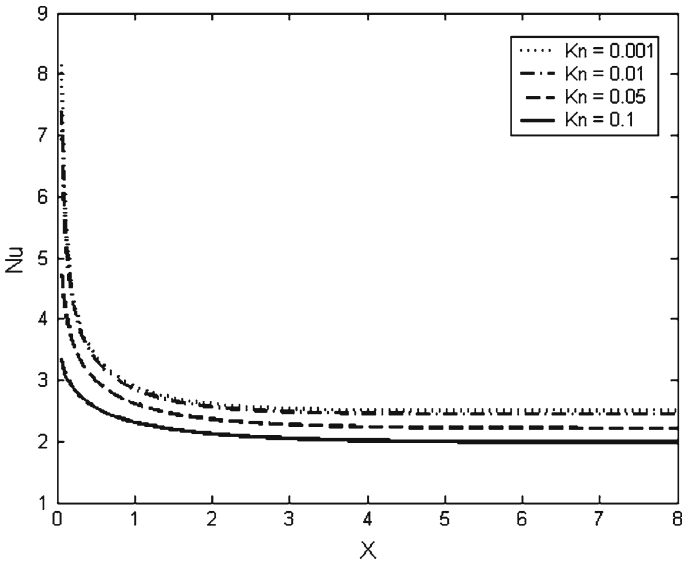

Fig. 9 Effect of Kn on Nu distribution: Da = 1, Γ = 10, Pe = 100, Bi = 1, K_R = 1

at the wall. As a result, the adjacent fluid to the wall does not feel the real temperature of the wall. This results in lower heat flux from the wall to the fluid and so Nusselt number decreases. The reduction in Nu due to the increase in temperature jump dominates the increase in Nu due to the increase in fluid flow rate and as a net result, Nu decreases as Kn increases.

Figure 10 shows the effect of Darcy number on local Nusselt number distribution. It can be noted that there are two opposite trends in the effect of Darcy number

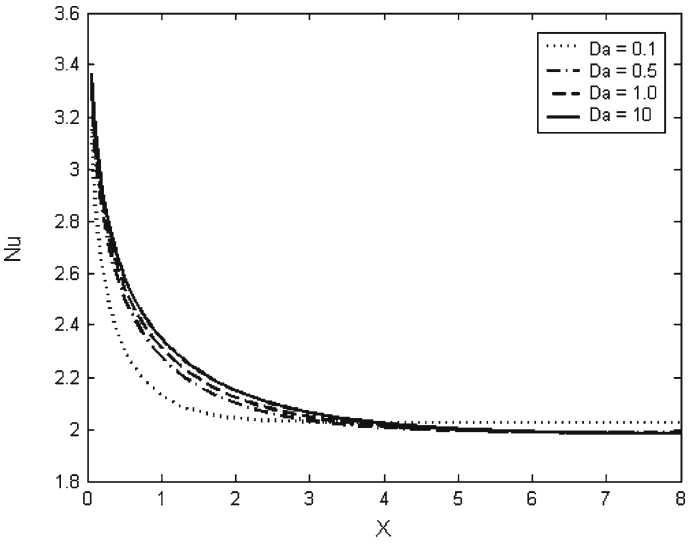

Fig. 10 Effect of Da on Nu distribution: Kn = 0.1, $\Gamma = 10$, Pe = 100, Bi = 1, $K_R = 1$

on Nusselt number in the developing and fully developed regions. As Darcy number increases, both velocity slip and temperature jump increases causing Nusselt number to increase and decrease, respectively. The effect of Da on velocity slip dominates the effect of Da on temperature jump within the developing region. The net effect is an increase in Nu with Da within this region (due to the increase in gas flow rate which causes more absorption for the heat from the wall). However, the effect of Da on temperature jump dominates its effect on velocity slip within the fully developed region. The net effect is a decrease in Nu number as Da increases within this region (due to the increase in temperature jump which reduces the amount of heat transfer from the wall to the fluid). Also, one may observe that the effect of Darcy number on Nusselt is insignificant at large values of X. In addition, the thermal entrance length increased with Darcy number.

Figure 11 shows the effect of Forchheimer number on local Nusselt number distribution. It can be noted that there are two opposite trends in the effect of Forchheimer number on Nusselt number in the developing and fully developed regions. As Forchheimer number increases, then both velocity slip and temperature jump decrease causing Nusselt number to decrease and increase, respectively. The effect of Γ on velocity slip is more significant in the developing region as compared with its effect on the temperature jump. As a result, increasing Γ has the effect of decreasing Nu due to the reduction in gas flow rate. The reduction in gas flow rate causes a reduction in the amount of heat transfer from the wall to the fluid. Now, in the fully developed region, the effect of Γ on temperature jump is more significant as compared to its effect on velocity slip. As a result, increasing Γ leads to an increase in Nu due to the reduction in temperature jump at the wall. This reduction in temperature jump increases the rate of heat transfer from the wall to the fluid. Also, one may observe that the effect of Forchheimer number on Nusselt number is relatively insignificant at large values of X. In addition, the thermal entrance length increased as Forchheimer number is decreased.

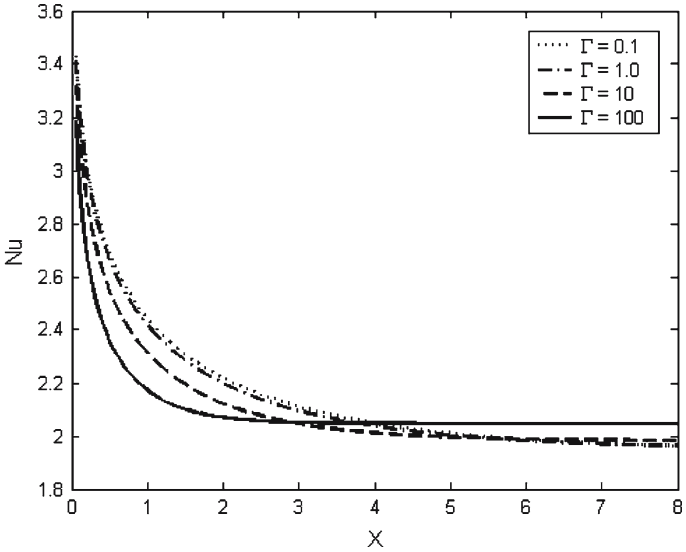

Fig. 11 Effect of Γ on Nu distribution: Kn = 0.1, Da = 1, Pe = 100, Bi = 1, $K_R = 1$

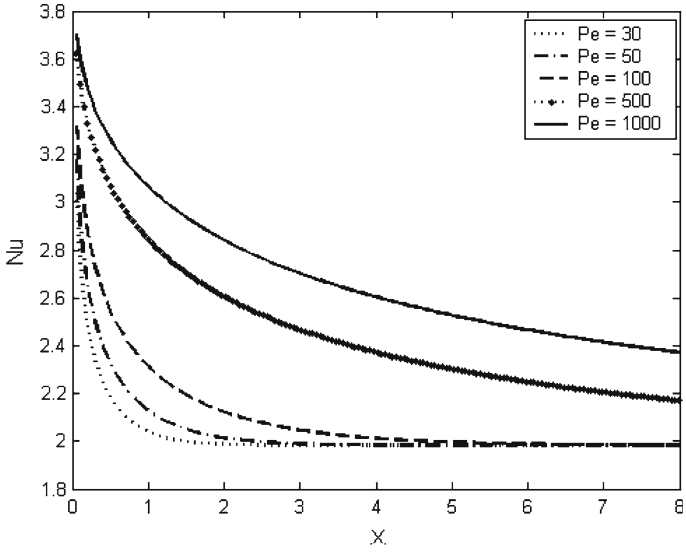

Fig. 12 Effect of Pe on Nu distribution: Kn = 0.1, Da = 1, Γ = 10, Bi = 1, $K_R = 1$

Figure 12 shows the effect of Peclet number on local Nusselt number distribution. It can be noted that as Peclet number increases the Nusselt number increases. This increase in heat transfer is due to the decrease in temperature jump at the wall. The effect of Peclet number on Nusselt number is less significant at large values of X. On the other hand, the thermal entrance length increased with Peclet number.

To explain why the effect of Γ, Da, and Pe numbers on Nusselt number is insignificant at large X, we need to note that at large X: $\partial\theta_f/\partial X \approx 0$ as the flow becomes fully

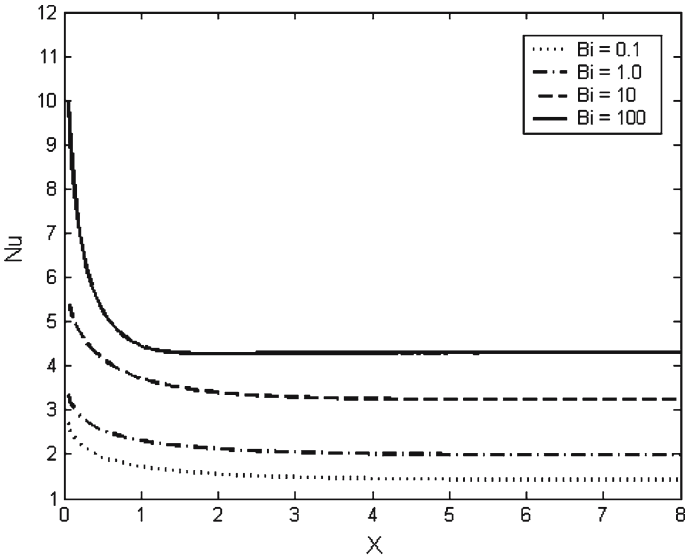

Fig. 13 Effect of Bi on Nu distribution: Kn = 0.1, Da = 1, $\Gamma = 10$, Pe = 100, $K_R = 1$

developed thermally. This term is multiplied by U and Pe in the energy equation (2), and both Γ and Da, affect U directly and not θ_f. Therefore, if U and Pe disappear as $\partial\theta_f/\partial X$ disappears then Γ, Da and Pe will have no effect on θ_f and hence on Nu.

Figure 13 shows the effect of Biot number on local Nusselt number distribution. It can be noted that as Biot number increases, the Nusselt number increases. This increase in Nusselt number is due to the increase in heat transfer between the fluid and solid media, which leads to increased heat transfer from the wall to both domains and so Nusselt number is increased. Also, increasing Biot number decreases temperature jump at the wall and this causes an increase in Nusselt number. On the other hand, the thermal entrance length increases as Biot number decreases.

Figure 14 shows the effect of conduction coefficient ratio K_R on local Nusselt number distribution. It can be noted that as K_R increases, the Nusselt number decreases. As K_R increases, the resistance of the solid phase to heat transfer becomes larger than that in the fluid phase and this lowers the heat transfer from the wall. As a result, Nusselt number decreases. Also as K_R increases, the temperature jump at the wall increases due to the reduction in thermal conductivity of the solid. This in turn causes an imperfect thermal contact between the solid domain and the wall. The increase in thermal resistance between the solid domain and the wall causes noticeable reduction in Nusselt number. We also note that although the fluid thermal conductivity increased, this did not cause any improvement in Nu due to the existing temperature jump at the wall.

5 Conclusions

The present numerical solutions are carried out for the case of steady laminar forced convection slip-flow between semi-infinite parallel-plates porous micro-channel under

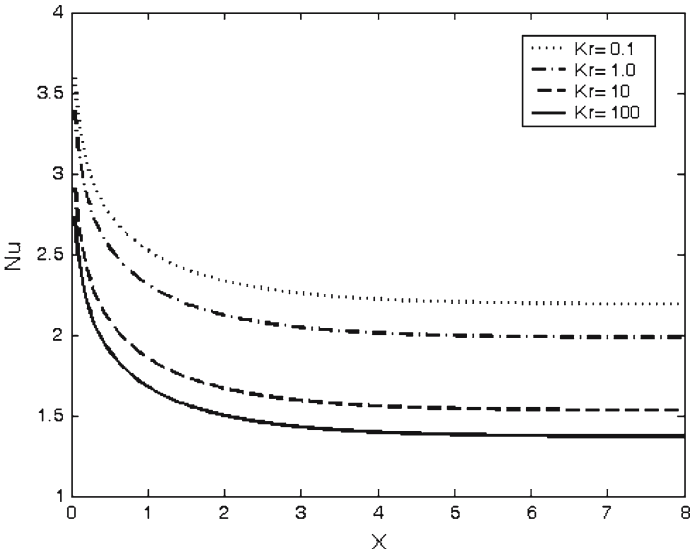

Fig. 14 Effect of K_R on Nu distribution: Kn = 0.1, Da = 1, $\Gamma = 10$, Pe = 100, Bi = 1

LTNE conditions. In this study, the slip-flow regime ($0.001 \leq \mathrm{Kn} \leq 0.1$) is considered and the Darcy–Brinkman–Forchheimer model is used to model the flow inside the porous domain. The present study reports the effect of several operating parameters on the velocity slip and temperature jump at the wall. Mainly, the current study demonstrates the effects of: Kn, Da, Γ, Pe, Bi, and K_R. Results are given in terms of skin friction ($C_f Re^*$) and local Nusselt number (Nu).

The skin friction is found to (1) increase as Darcy number increases, (2) decreases as Forchheimer number or Knudsen number increases. On the other hand, Nusselt number is found to (1) decrease as Knudsen number, Forchheimer number, or K_R increases. (2) increase as Peclet number, Darcy number, or Biot number increases.

Also, it is found that the solid and fluid non-dimensional temperatures approach each other when Γ, Bi and K_R increase, and when Da and Pe decrease. In addition, it was observed that the flow thermal entrance length is shorter if Bi, Γ and K_R increase or if Kn, Da, and Pe decrease.

Appendix

To validate the model equations used in this paper, the following analysis is presented: Following Bejan (2004), the fluid flow in porous domain is simulated as a fluid flowing in bundle of straight macro-tubes. The velocity distribution in each macro-tube, after neglecting the inertial forces, is governed by the following momentum equation and boundary conditions

$$\frac{1}{r}\frac{\partial}{\partial r}\left(r\frac{\partial u}{\partial r}\right) = \frac{1}{\mu}\frac{\partial p}{\partial x} \tag{12}$$

$$\frac{\partial u}{\partial r}(0) = 0, \quad u(r_0) = 0 \tag{13}$$

therefore, the velocity distribution is given as

$$u(r) = -\frac{1}{4\mu}\frac{\partial p}{\partial x}(r_0^2 - r^2) \tag{14}$$

Now, conducting the volume averaging on each tube, by integrating the velocity distribution over the tube cross-sectional area and dividing the result by the cross-sectional area, we get the following expression for the average velocity

$$U = -\frac{1}{8\mu}\frac{\partial p}{\partial x}r_0^2 \tag{15}$$

Comparing this with Darcy model

$$U = -\frac{K}{\mu}\frac{\partial p}{\partial x} \tag{16}$$

where K is the permeability, yields the following expression for the permeability K of the macro-porous-tube:

$$K = \frac{r_0^2}{8} \tag{17}$$

By repeating the same analysis, assuming each macro-tube now is a micro-tube. The velocity distribution is now governed by the following momentum equation, symmetry and velocity slip boundary conditions

$$\frac{1}{r}\frac{\partial}{\partial r}\left(r\frac{\partial u}{\partial r}\right) = \frac{1}{\mu}\frac{\partial p}{\partial x} \tag{18}$$

$$\frac{\partial u}{\partial r}(0) = 0, \quad u(r_0) = -\left(\frac{2-\sigma_v}{\sigma_v}\right)\lambda\frac{\partial u}{\partial r}(r_0) \tag{19}$$

where σ_v is the tangential momentum accommodation coefficient and λ is the mean free path of the fluid molecules. Equations (7) and (8) are solved to yield the following velocity distribution in the micro-tubes

$$u(r) = \frac{1}{\mu}\frac{\partial p}{\partial x}\frac{r^2}{4} - \frac{1}{\mu}\frac{\partial p}{\partial x}\frac{r_0^2}{4}\left(1 + 2\left\{\frac{2-\sigma_v}{\sigma_v}\right\}\mathrm{Kn}\right) \tag{20}$$

Applying the volume averaging on this velocity distribution to get the average velocity U as

$$U = -\frac{1}{\mu}\frac{\partial p}{\partial x}\frac{r_0^2}{8}\left(1 + 4\left\{\frac{2-\sigma_v}{\sigma_v}\right\}\mathrm{Kn}\right) \tag{21}$$

where here $\mathrm{Kn} = \lambda/r_0 =$ Knudsen number.

Comparing this expression for U with that described by Darcy model as in Eq. (4) yields the following expression for the permeability, K:

$$K = \frac{r_0^2}{8}\left(1 + 4\left\{\frac{2-\sigma_v}{\sigma_v}\right\}\mathrm{Kn}\right) \tag{22}$$

Note that the permeability of the micro-porous channel is higher than that of the macro-porous channel due to the slip at the interface between the fluid and the solid surfaces of the pores (i.e., the tubes walls in the simplified simulation). The presence

of slip allows more fluid flow through the channel under the effect of the same driving pressure gradient dp/dx.

Also, note that the fluid flow in both the macro and the micro-channels (after neglecting inertial forces) is described by the same Darcy model which has the same form

$$U = -\frac{K}{\mu}\frac{\partial p}{\partial x} \tag{23}$$

and the only difference between the two cases (macro- and micro-channels) is in the definition of the modified permeability K which is

$$\text{for macro-channel: } K = \frac{r_0^2}{8} \tag{24}$$

$$\text{for micro-channel: } K = \frac{r_0^2}{8}\left(1 + 4\left\{\frac{2-\sigma_\mathrm{v}}{\sigma_\mathrm{v}}\right\}\mathrm{Kn}\right) \tag{25}$$

Note that each model predicts the same permeability $K = r_0^2/8$ when $\mathrm{Kn} = 0$. Also, note that for the macro porous channel, the permeability depends on the geometrical aspects of the channel, while for the case of micro porous channel, it depends on the geometrical aspects of the channel, the accommodation coefficient of the pore surface (σ_v) and Knudsen number ($\mathrm{Kn} = \lambda/r_0$), which itself depends on the mean free path length of the gas molecules and r_0.

In conclusion, we believe that the same governing equations (Darcy–Brinkman–Forchheimer momentum and the energy equations) which are usually used in macro channel situations are still valid for micro channel situations but under the condition of using new values of the parameters that resulted from the interaction between the fluid and solid domains. Examples of these parameters are the permeability K, effective viscosity μ_eff, Forchheimer term F, etc.... Note here that we do not talk about the pure fluid properties but about the interaction properties between fluid and solid. We here refer the reader to the work of Tang et al. (2005) which supports our conclusion.

References

Ameel, T.A., Barron, R.F., Wang, X.M., Warrington, R.O.: Laminar forced convection in a circular tube with constant heat flux and slip flow. Microscale Thermophys. Eng. **1**, 303–320 (1997)

Arkilic, E.B., Breuer, K.S., Schmidt, M.A.: Gaseous flow in microchannels, application of microfabrication to fluid mechanics, ASME FED **197**, 57–66 (1994)

Barber, R.W., Emerson, D.R.: A numerical investigation of low Reynolds number gaseous slip flow at the entrance of circular and parallel plate microchannels. Proceedings of the ECCOMAS Computational Fluid Dynamics Conference, Swansea, Wales, UK (2001)

Barron, R.F., Wang, X.M., Warrington, R.O., Ameel, T.A.: Evaluation of the eigenvalues for the Graetz problem in slip-flow. Int. Commun. Heat Mass Trans. **23**, 563–574 (1996)

Barron, R.F., Wang, X.M., Ameel, T.A., Warrington, R.O.: The Graetz problem extended to slip flow. Int. J. Heat Mass Trans. **40**, 1817–1823 (1996)

Bejan, A.: Editorial, J. Porous Media **1**, i–ii (2000)

Bejan, A.: Convection Heat Transfer, 3rd edn. Chapter 12, John-Wiley, New York (2004)

Beskok, A., Karniadakis, G.E.: Simulation of heat and momentum transfer in complex micro geometries, J. Thermophys. Heat Trans. **8**(4), 647–653 (1994)

Eckert, E.G.R., Drake, R.M.: Analysis of Heat and Mass Transfer, pp. 467–486. McGraw-Hill, New York (1972)

Gad-El-Hak, M.: The fluid mechanics of microdevices—The Freeman scholar lecture, J. Fluids Eng. **121**, 5–33 (1999)
Haddad, O.M., Al-Nimr, M.A., AbuZaid, M.M.: The effect of frequency of fluctuating driving force on basic gaseous micro-flows. Acta Mechanica **179**, 249–259 (2005a)
Haddad, O.M., AbuZaid, M.M., Al-Nimr, M.A.: Developing free convection gas flow in a vertical open-ended micro-channel filled with porous media. Numer. Heat Trans. Part A **48**, 693–710 (2005b)
Haddad, O.M., Al-Nimr, M.A., Taamneh, Y.: Hydrodynamic and thermal behavior of gas flow in micro-channels filled with porous media. Accepted for publication in J. Porous Media (2006a)
Haddad, O.M., Al-Nimr, M.A., AbuZaid, M.M.: The effect of periodically oscillating driving force on basic micro flows in porous media. Accepted for publication in J. Porous Media (2006b)
Hoffman, J.D.: Numerical Methods for Engineers and Scientists. Marcel Dekker, New York (2001)
Larrode, F.E., Housiadas, C., Drossinos, Y.: Slip-flow heat transfer in circular tubes. Int. J. Heat Mass Trans. **43**, 2669–2680 (2000)
Liu, J.Q., Tai, Y.C. and Ho, C.M.: MEMS for pressure distribution studies of gaseous flows in micro-channels. Proc. IEEE Micro-electromech. Syst. 209–215 (1995)
Marafie A., Vafai K.: Analysis of non-Darcian effects on temperature differentials in porous media. Int. J. Heat Mass Trans. **44**, 4401–4411 (2001)
Shih, J.C., Ho, C., Liu, J., Tai Y.: Monatomic and polyatomic gas flow through uniform microchannels. Microelecromech. Syst. (MEMS) **59**, 197–203 (1996)
Shih, Y.P., Huang, C.C., Tsay, S.Y.: Extended Leveque solution for laminar heat transfer to power-law fluids in pipes with wall slip. Int. J. Heat Mass Trans. **38**, 403–408 (1995)
Tang, G.H., Tao, W.Q., He, Y.L.: Gas slippage effect on microscale porous flow using the lattice Boltzmann method. Phys. Rev. E **72**(56301), 1–8 (2005)
Wang, M.L., Ameel, T.A., Frazier, A.B., Warrington, R.O.: Microtube convection heat transfer for a power-law fluid in laminar slip flow with an isoflux boundary condition. Int. Mechanical Eng. Congress and Exposition, Anaheim, CA, HTD-Vol. 361–3, pp. 157–164 (1998)
Wang, X. M.: Evaluation of the eigenvalues of the Graetz problem in slip-flow. M.Sc. Thesis, Louisiana Tech. University, Ruston, Louisiana (1996)
Yu, S.P., Ameel, T.A.: Slip flow low Peclet number thermal entry problem within a flat microchannel subject to constant wall temperature. Proceedings of the Conference on Heat Transfer and Transport Phenomena in Microsystems, Banff, Alta, Canada (2000)
Yu, S.P., Ameel, T.A.: Slip-flow heat transfer in rectangular microchannels. Int. J. Heat Mass Trans. **44**, 4225–4234 (2001)